Pulse measurements by randomly quasi phase matched second harmonic generation in the regime of total internal reflection

2009 J. Phys. B: At. Mol. Opt. Phys. 42 175403

(http://iopscience.iop.org/0953-4075/42/17/175403)

J. Phys. B: At. Mol. Opt. Phys. **42** (2009) 175403 (4pp) doi:10.1088/0953-4075/42/17/175403

Pulse measurements by randomly quasi phase matched second harmonic generation in the regime of total internal reflection

David Dumay[1], Solomon M Saltiel[1,2], Dragomir N Neshev[1], Wieslaw Krolikowski[1] and Yuri S Kivshar[1]

[1] Nonlinear Physics Centre and Laser Physics Centre, Research School of Physics and Engineering, Australian National University, Canberra ACT 0200, Australia
[2] Department of Physics, Sofia University 'St Kl Ohridski', 1164 Sofia, Bulgaria

E-mail: Dragomir.Neshev@anu.edu.au

Received 4 June 2009, in final form 16 July 2009
Published 20 August 2009
Online at stacks.iop.org/JPhysB/42/175403

Abstract
We demonstrate experimentally the frequency doubling in disordered quadratic nonlinear media in the regime of total internal reflection of the fundamental beam. We show how the transversely emitted second harmonic can be employed for an efficient characterization of short laser pulses.

(Some figures in this article are in colour only in the electronic version)

Wavelength conversion of light via second-harmonic generation (SHG) is probably the best known nonlinear optical processes, finding numerous applications in both fundamental science and technology. One of the most prominent applications of this process is the measurements of short laser pulses. For such measurements, SHG enables optical gating of one pulse with another [1], to obtain auto- or cross-correlation signal. To realize such optical gating, two pulses with a variable time delay have to be utilized. These pulses can be obtained by splitting the initial laser beam into two replicas; however, such splitting and the consequent timing of the pulses require a number of optical and mechanical elements. Typical pulse-characterization techniques include autocorrelation [2], frequency resolved optical gating (FROG) [3] or spectral phase interferometry for direct electric-field reconstruction (SPIDER) [4]. The recent advances of pulse measurements have also led to new, simpler and single beam instruments, such as grating-eliminated no-nonsense observation of ultrafast incident laser light e-fields (GRENOUILLE) [5], phazzler [6, 7] and multiphoton intrapulse interference phase scan (MIIPS) [8]. However, the instruments based on these techniques still require expensive elements such as pulse shapers and are destructive: the pulses cannot be used during the measurements.

Here, we propose and demonstrate a pulse autocorrelation scheme, achieved with a single beam only and no delay line. In addition, the output of our scheme can be fully reused while measurements are performed. This technique relies on the effect of *transverse SHG* in a crystal with a random distribution of its ferroelectric domains under the regime of total internal reflection (TIR). We analyse in details this process and derive the operational conditions of this technique.

To achieve efficient conversion of a fundamental wave (FW) beam into a second harmonic (SH), one needs to match their phase velocities in the medium. This requires satisfying the so-called phase matching (PM) condition. PM can often be achieved in bulk crystals by utilizing the crystalline birefringence. However, there are crystals and wavelength ranges where this method cannot be applied. For such media alternative methods have been developed to compensate for the resulting phase mismatch $\Delta k = k_2 - 2k_1$, where k_2 and k_1 are the wavevectors of the SH and the FW, respectively. Already in the pioneering paper of Armstrong *et al* [9], two fundamental approaches for achieving efficient frequency conversion based on the so-called quasi phase matching (QPM) have been suggested: (i) alternation of the ferroelectric domains of a ferroelectric crystal and (ii) multiple TIRs at the crystal

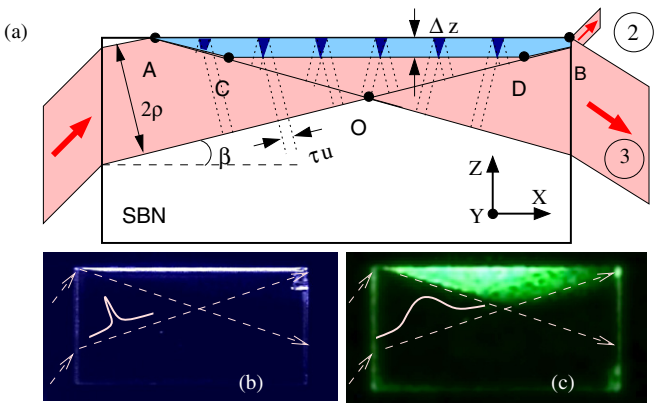

Figure 1. (a) Interaction geometry of transverse SHG when the fundamental beam is totally reflected from the crystal surface. Experimentally recorded SH emission in the case of (b) short (200 fs) and (c) long (10 ps) laser pulses.

boundaries. Both of these methods have only been applied independently as PM techniques.

In our approach, we utilize the combined operation of QPM and TIR. Namely, we show that the TIR in the case of randomly quasi-phase-matched SHG [10] leads to a four-fold increase in the SHG efficiency and provides an efficient mean for measurement of ultrashort pulses.

The effect of random QPM can be observed in many naturally grown crystals that are known to exhibit disordered distribution of micro- and nano-size domains, with a typical example being the strontium barium niobate (SBN) crystal. Such a random domain distribution automatically fulfils the PM conditions for any parametric process, independent of the geometry of the pump beams or operating wavelength. This unique property has been used in a number of works, starting with the first observation of single colour SHG in a SBN crystal [11], followed by the demonstration of multi-colour random QPM SHG [12, 13], conical SHG [14] and multi-colour laser conversion [15, 16]. In addition, broadband spectral mapping of laser pulses [17] and autocorrelation measurement of short pulses [18] have been recently demonstrated.

In the geometry of TIR, the FW beam enters the crystal at an angle $+\beta$, being totally reflected from the inner surface, as shown in figure 1(a). Here, $\beta < \beta_{\mathrm{TIR}} = \cos^{-1}(1/n)$, where n is the refractive index at the fundamental wavelength. As a result, this geometry provides two effective beams: incident (I) and reflected beam (R), the reflected beam propagating at an angle $-\beta$. In the area of overlap, these two noncollinear fundamental beams (intersecting at angle 2β) generate a SH signal, emitted transversely to the beams (perpendicular to the plane of figure 1(a)). The intensity of this emission is four times larger than that generated by a single beam due to the doubling of the total light intensity in the area of beam overlap. We study this effect with two different laser sources: (i) femtosecond Ti:Sapphire oscillator (Mira, Coherent) at $\lambda = 0.81$ μm, with pulse width $\tau \simeq 200$ fs, a repetition rate of 76 MHz, an average power of ~400 mW and a peak power of ~26 kW; and (ii) mode-locked picosecond Nd:YVO laser with a regenerative amplifier at $\lambda = 1.053$ μm, $\tau \simeq 10$ ps, a repetition rate of 20 Hz, an average power of ~1 mW and a peak power of ~5 MW. We demonstrate that the width of the SH trace can be used to estimate the laser pulse duration.

In our experiments, we use a $10 \times 5 \times 5$ mm unpoled SBN crystal with all faces polished. The reflecting surface is chosen to be perpendicular to the Z-axis of the crystal, and the incident and reflected beams propagate in the (X, Z)-plane at angles $\pm\beta$ to the X-axis, respectively. The incident FW and the emitted SH beams are both polarized along the crystallographic axis Z. The incident beam is mildly focused in the vertical direction by a cylindrical lens to a spot of 1 mm $\times$ 100 μm in order to increase the effective intensity inside the crystal.

It is clear that, due to the overlap of the incident and reflected beams, the 'thickness' of the area of planar emission differs significantly for the two cases of short and long pulses. This is a direct consequence of the fact that the emission region is determined by overlap of the pulses as well as the beams. For short pulses, the incident and reflected pulses overlap only in a narrow area close to the reflecting surface, as illustrated in figure 1(a). Therefore, the region of the SH emission is confined to the polygon 'ABDC'. On the other hand, for long pulses the emission region is defined mainly by the overlap of the beams which is the triangle 'ABO'. In figures 1(b) and (c) we show two typical images for TIR-SH emission, in the case of short (~200 fs) and long (~10 ps) input pulses, respectively. The width Δz of the SH emission region is directly related to the pulse duration τ (see e.g. [19]). If we assume a Gaussian pulse shape, then

$$\Delta z = \tau u/(2\sqrt{2}\sin\beta), \tag{1}$$

where u is the speed of light inside the SBN crystal. The smaller the angle β, the wider the autocorrelation trace. The crossing point 'O' will change for different incident angles and it can be located inside the crystal, at the output facet, or even behind it. As equation (1) shows, the correct measurement of short pulses requires that the thickness of the overlap of the beams be at least three times larger than Δz. From this condition, we find that the angle β cannot be smaller than the critical angle β_{cr} defined by the equation

$$\sin\beta_{\mathrm{cr}}\tan\beta_{\mathrm{cr}} = \tau u/L, \tag{2}$$

where L is the crystal length. For example, equation (2) predicts that for $\tau = 200$ fs and $L = 1$ cm the input angle should be larger than $\beta_{\mathrm{cr}} = 3^\circ$.

The PM conditions (figure 2) define the shape of the SH emission (planar and conical). For the SH planar emission in the (X, Y)-plane, as illustrated in figure 2(a), the PM is determined by the relation

$$\vec{k}_{1I} + \vec{k}_{1R} + \vec{G}_i = \vec{k}_2, \tag{3}$$

where I, R correspond to incident and reflected beams, respectively, and $\vec{G}_i$, $i = 1 \cdots \infty$ are the grating vectors of the domain distribution available in the crystal. In addition, the PM conditions for the conical SH emission along the direction Z are shown in figure 2(b) and defined as

$$2\vec{k}_1 + \vec{G}_1 = \vec{k}_2, 2\vec{k}_1 - \vec{G}_2 = \vec{k}_2. \tag{4}$$

Here $\vec{G}_1$ and $\vec{G}_2$ are grating vectors from the pool of grating vector distribution that have the same length and lie in the

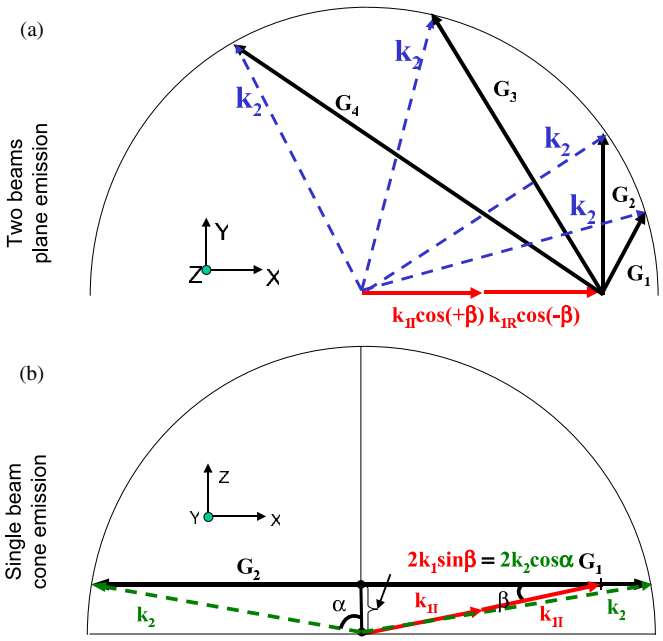

Figure 2. Schematic phase matching diagrams for: (a) planar SH from the incident (I) and the reflected (R) beam. (b) Conical SH emission from the incident beam. G_i correspond to the available grating vectors of the nonlinear photonic structures due to the random domain distribution in the SBN crystal.

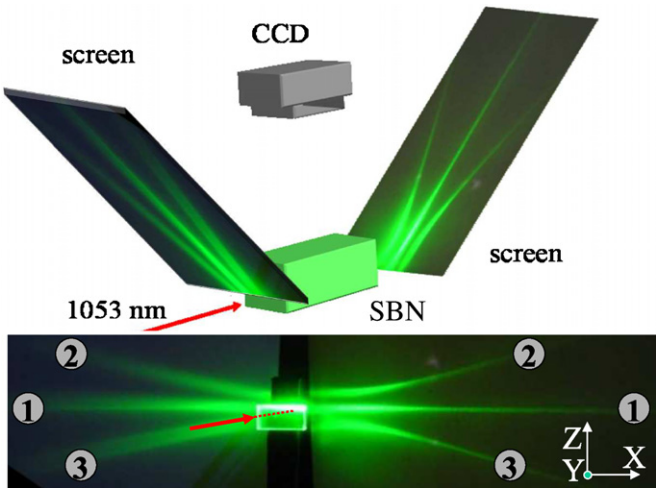

Figure 3. Emission of SH light in forward, transverse and backward directions. (top)—3D representation; (bottom)—top view. (1) marks the trace from the planar SH emission, (2) and (3)—cone sections on the screen marking the SH conical emission from the input beam and its reflected replica, respectively.

X, Y-plane, to satisfy the PM conditions (figure 2(b)). Equations (4) split into two PM conditions, longitudinal and transverse ones. The transverse phase matching is always fulfilled due to the disordered distribution of the domain sizes [13, 16, 20]. The longitudinal phase matching defines the SH cone angle and depends on the beam orientation in the (X, Z)-plane,

$$\cos\alpha = (2k_1/k_2)\sin\beta. \tag{5}$$

For the case when the fundamental beam propagates along $X(\beta = 0)$, the cone angle is 90° resulting in a planar emission. In our experiments, the two beams, inclined symmetrically with respect to the X-axis, act as an equivalent fundamental beam directed along X. This virtual beam then generates SH in the form of a plane perpendicular to the crystal axis Z. We note that this type of emission is similar to that reported earlier in [19]; however due to the TIR, there is no splitting of the input energy into two beams. Hence, the current geometry offers a substantial increase in the emitted SH signal.

Figure 3 shows the SH emission under the TIR geometry, realized with the higher peak power pulses of 10 ps, in order to improve the visibility of the SH emission. The SH signal has three spatially resolved contributions. The middle line (1) is due to the combined action of incident and reflected beams, which results in emission in all directions in the (X, Y)-plane. Independently, each beam (incident and reflected) emits SH in a cone, centred around the axis Z and marked as (2) and (3). The direction of the SH conical wave generated by the incident beam coincides with the direction $+Z$, while that generated by the reflected beam, with the direction $-Z$. If we compare the intensity of the SH light emitted due to a combined action of the two fundamental beams and the SH generated from a single beam, the SH emission from the two beams is much stronger than the SH from a single beam. Accurate measurements show that the combined beam SH intensity is 3.8 times higher. This agrees qualitatively with the expected four times increase in the SH intensity when the FW intensity is doubled near the surface.

It can also be seen from figure 3(bottom) that emission in the forward and backward directions show comparable efficiencies. Both, right and left hyperbolas (2 and 3) have comparable intensities in the forward and backward directions. Measuring the SH intensity in both directions at equal distances from the crystal gives an intensity ratio of 4:3. This result cannot be explained by the reflection of the forward radiation from the output surface, hence it suggests the presence of strong backward SHG.

Very importantly, the SH from the mixing of the two fundamental beams, emitted in the transverse direction, appears useful for monitoring the pulse duration through recording of the width of the planar emission. This width of the area of beam overlap is related to the pulse duration by equation (1). This is a unique situation for pulse measurements since temporal information about the pulse is obtained with a single input beam only, without necessity of a delay line and external beam splitting.

To demonstrate this concept, we record the emission traces in the transverse direction for the femtosecond 810 nm pulses, at three different values of the internal angle β. The digitized profiles (recorded close to the output face of the crystal) are depicted in figure 4(a). These asymmetric profiles in fact represent only a half of the fully symmetric autocorrelation function. The three profiles obviously have different spatial widths due to the difference in the effective time delay for the different inclination angles. These spatial intensity distributions can be converted to temporal ones through the relation $t = 2zn\sin\beta/c$, where n is the refractive index of the SBN crystal for the fundamental wavelength [21]. As shown in figure 4(b), all the three autocorrelation functions have the same width (within 10% experimental error). The

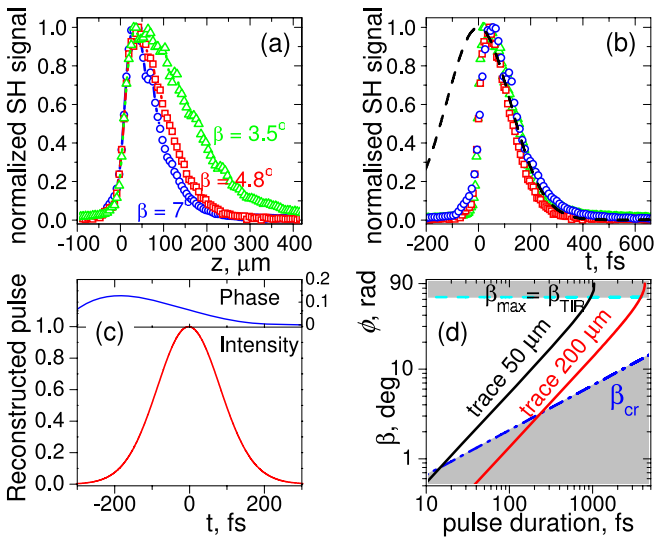

Figure 4. (a) Pulse autocorrelation profiles measured for three different incident (internal) angles of the fundamental beam. (b) A comparison of the autocorrelation functions measured for the three inclination angles (as in (a)) and the recovered autocorrelation trace from the GRENOUILLE (black dashed line). (c) FROG reconstructed intensity (bottom) and phase (top) of the incident pulse, showing Gaussian pulses of FWHM of 200.56 fs. (d) A plot describing the choice of the internal incident angle β (in degrees) as a function of pulse duration.

difference in the width can be attributed to the inaccuracy of the internal angle β measurement and to the different temporal dispersion inside the crystal. The obtained average full width at half-maximum (FWHM) of the autocorrelation function is 284.3 fs and agrees well with the value of 288.4 fs obtained independently from a GRENOUILLE measurement [5]. The shape of the autocorrelation function obtained by the GRENOUILLE is shown in figure 4(b) with a dashed line. In addition to the autocorrelation, the FROG measurement enables a complete pulse reconstruction that is shown in figure 4(c). The reconstructed pulse has a FWHM of 200.6 fs and a Gaussian shape ($R^2 = 0.9999$). Our result on the pulse duration measurement obtained with equation (1) slightly overestimates the pulse width, giving an average pulse duration of 228 fs. This discrepancy is most likely due to slight chirp of the pulse, as seen in figure 4(c)-top.

An important characteristic of our device is the range of the pulse duration that is possible to resolve experimentally. As discussed earlier, the pulse duration that can be measured is limited from below by the resolution of the imaging system, while the upper limit is defined by the critical angle of TIR (β_{TIR}) and the beam width (equation (2)). In figure 4(d), we give an estimate for the proper choice of the internal angle β as a function of the pulse duration. The resolution of the imaging system is defined as a solid line (equation (1)), shown for two trace thicknesses of 50 and 200 μm. For example, figure 4(d) shows that if the imaging system is not capable of resolving lines below 200 μm, one cannot expect to monitor pulses shorter than 250 fs or alternatively no longer than 2 ps. As such, the working range is confined to the white area between the two shaded regions in figure 4(b) and to the right of the image resolution line.

In conclusion, we have demonstrated SHG in disordered quadratic nonlinear media assisted by TIR of the fundamental wave and have shown that this effect can be employed for characterization of short laser pulses. In this TIR geometry, we have observed nearly a four-fold increase in the SHG efficiency in comparison with the scheme of beam splitting used in [19]. We believe that the suggested geometry provides one of the simplest schemes for pulse monitoring that requires only a single beam, a nonlinear crystal and a simple camera. Such a nondestructive monitoring technique enables integration inside a laser or in an optical system without disturbing its operation.

Acknowledgments

This work was supported by the Australian Research Council. SS thanks the Australian National University for hospitality and support.

References

[1] Trebino R 2002 *Frequency-Resolved Optical Gating: The Measurement of Ultrashort Laser Pulses* (Boston, MA: Kluwer)
[2] Weber H P 1967 *J. Appl. Phys.* **38** 2231
[3] Kane D J and Trebino R 1993 *Opt. Lett.* **18** 823
[4] Anderson M E, Monmayrant A, Gorza S-P, Wasylczyk P and Walmsley I A 2008 *Laser Phys. Lett.* **5** 259
[5] O'Shea P, Kimmel M, Gu X and Trebino R 2001 *Opt. Lett.* **26** 932
[6] Verluise F, Laude V, Cheng Z, Spielmann Ch and Tournois P 2000 *Opt. Lett.* **25** 575
[7] Monmayrant A, Joffre M, Oksenhendler T, Herzog R, Kaplan D and Tournois P 2003 *Opt. Lett.* **28** 278
[8] Coello Y, Lozovoy V V, Gunaratne T C, Xu B, Borukhovich I, Tseng C-H, Weinacht T and Dantus M 2008 *J. Opt. Soc. Am.* B **25** A140
[9] Armstrong J A, Bloembergen N, Ducuing J and Pershan P S 1962 *Phys. Rev.* **127** 1918
[10] Baudrier-Raybaut M, Haidar R, Kupecek Ph, Lemasson Ph and Rosencher E 2004 *Nature (Lond.)* **432** 374
[11] Kawai S, Ogawa T, Lee H S, DeMattei R C and Feigelson R S 1998 *Appl. Phys. Lett.* **73** 768
[12] Romero J J, Jaque D, García Solé J and Kaminskii A A 2002 *Appl. Phys. Lett.* **81** 4106
[13] Romero J J, Aragó C, Gonzalo J A, Jaque D and García Solé J 2003 *J. Appl. Phys.* **93** 3111
[14] Tunyagi A R, Ulex M and Betzler K 2003 *Phys. Rev. Lett.* **90** 243901
[15] Ramirez M O, Romero J J, Molina P and Bausa L E 2005 *Appl. Phys.* B **81** 827
[16] Molina P, Ramirez M O and Bausa L E 2008 *Adv. Funct. Mat.* **18** 709
[17] Fischer R, Neshev D N, Saltiel S M, Krolikowski W and Kivshar Yu S 2006 *Appl. Phys. Lett.* **89** 191105
[18] Fischer R, Neshev D N, Saltiel S M, Sukhorukov A A, Krolikowski W and Kivshar Yu S 2007 *Appl. Phys. Lett.* **91** 031104
[19] Roppo V, Dumay D, Trull J, Cojocaru C, Saltiel S, Staliunas K, Vilaseca R, Neshev D N, Krolikowski W and Kivshar Yu S 2008 *Opt. Express* **16** 14192
[20] Ramirez M O, Jaque D, Ivleva L and Bausa L E 2004 *J. Appl. Phys.* **95** 6185
[21] Woike Th, Granzow T, Dörfler U, Poetsch Ch, Wöhlecke M and Pankrath R 2001 *Phys. Status Solidi* A **186** R13